EPJ Web of Conferences **225**, 05003 (2020) https://doi.org/10.1051/epjconf/202022505003
ANIMMA 2019

The use of self-induced X-ray fluorescence in gamma-ray spectroscopy of uranium ore samples

T. Marchais[1]*, B. Pérot[1], C. Carasco[1], J-L. Ma[1], P-G. Allinei[1], H. Toubon[2], R. Goupillou[3], J. Collot[4]
[1] DEN/CAD/DTN/SMTA/LMN
[2] ORANO Mining
[3] SEPA/SET ORANO Mining
[4] Laboratory of Subatomic Physic and Cosmology, Université Grenoble Alpes, CNRS/IN2P3
* thomas.marchais@cea.fr

***Abstract* — Gamma logging for uranium exploration are currently based on total counting with Geiger Müller gas detectors or NaI (TI) scintillators. However, the total count rate interpretation in terms of uranium concentration may be impaired in case of roll fronts, when the radioactive equilibrium of the natural ^{238}U radioactive chain is modified by differential leaching of uranium and its daughter radioisotopes of thorium, radium, radon, etc. Indeed, in case of secular equilibrium, more than 95 % of gamma rays emitted by uranium ores come from ^{214}Pb and ^{214}Bi isotopes, which are in the back-end of ^{238}U chain. Consequently, these last might produce an intense gamma signal even when uranium is not present, or with a much smaller activity, in the ore. Therefore, gamma spectroscopy measurements of core samples are performed in surface with high-resolution hyper-pure germanium HPGe detectors to directly characterize uranium activity from the 1001 keV gamma ray of ^{234m}Pa, which is in the beginning of ^{238}U chain. However, due to the low intensity of this gamma ray, i.e. 0.84 %, acquisitions of several hours are needed. In view to characterize uranium concentration within a few minutes, we propose here a method using both the 92 keV gamma ray of ^{234}Th and the 98.4 keV uranium X-ray. This last is due to uranium self-induced fluorescence caused by gamma radiations of ^{214}Pb and ^{214}Bi, which create a significant Compton scattering continuum acting as a fluorescence source and resulting in the emission of uranium fluorescence X-rays. The comparison of the uranium activity obtained with the 92 keV and 98.4 keV lines allows detecting a uranium heterogeneity in the ore. Indeed, in case of uranium nugget, the 92 keV line leads to underestimated uranium concentration due to gamma self-absorption, but on the contrary the 98.4 keV line leads to an overestimation because of increased fluorescence. In order to test this new approach, several tens of uranium ore samples have been measured with a handheld HPGe FALCON 5000 detector.**

***Index Terms*— Self-induced X-ray fluorescence, gamma-ray spectroscopy, germanium detector, uranium mining, MCNP6**

I. Introduction

Current gamma measurements used to characterize the uranium content of ore samples are mainly based on two estimators. The first one is the total gamma count rate, which is approximately 90 % due to gamma radiations of ^{214}Pb and ^{214}Bi daughters (see further Fig. 1), in the back-end of ^{238}U chain. It allows short acquisition times but it is subject to potential imbalances in this decay chain. The second one is the 1001 keV gamma ray of ^{234m}Pa daughter in the beginning of ^{238}U chain, which is therefore not subject to a potential disequilibrium of the decay chain. Moreover, the sample mineralogy has little impact on attenuation of this radiation with a relatively high energy. However, its emission intensity is very small (0.847%) and its detection requires acquisition times of several hours, see Fig. 1. The objective of this study is to measure uranium content using more intense lines at lower energy, i.e. the 92 keV gamma ray of ^{234}Th and ^{235}U, and the 98 keV line due to uranium self-induced fluorescence (and to a lesser extend to a ^{234m}Pa gamma ray). This study is performed with samples of crushed ore filling a PVC holder. The gamma spectra are measured with a Falcon 5000 [1] handheld spectrometer from Mirion-Canberra, equipped with a HPGe planar detector (BEGE 2830 model). The method is studied by MCNP6 Monte Carlo calculation by the Nuclear Measurement Laboratory of CEA, DEN, Cadarache, and validated with experimental data obtained by ORANO Mining during a measurement campaign intended to characterize uranium content and imbalance of the samples [2].

The two rays at 92 keV and 98 keV are systematically present with a high intensity on uranium ore spectra (see example of a small concentration sample in Fig. 1), which makes it possible to envisage a significant measurement time reduction with respect to 1001 keV line.

II. Analysis of the gamma spectrum

A. Typical gamma spectrum of a uranium ore sample

Fig. 1 shows a typical HPGe high-resolution gamma spectrum of a real ore sample with a 419 ppm uranium concentration. The experimental setup is described further in Section II. In this section, we develop the theoretical formulae used to determine the uranium concentration from the net area of 1001 keV, 92 keV and 98 keV peaks, respectively. The concentration obtained with the 1001 keV gamma ray is considered in this work as the reference because it is less sensitive to attenuation effects compared to the two other low-energy radiations.

© The Authors, published by EDP Sciences. This is an open access article distributed under the terms of the Creative Commons Attribution License 4.0 (http://creativecommons.org/licenses/by/4.0/).

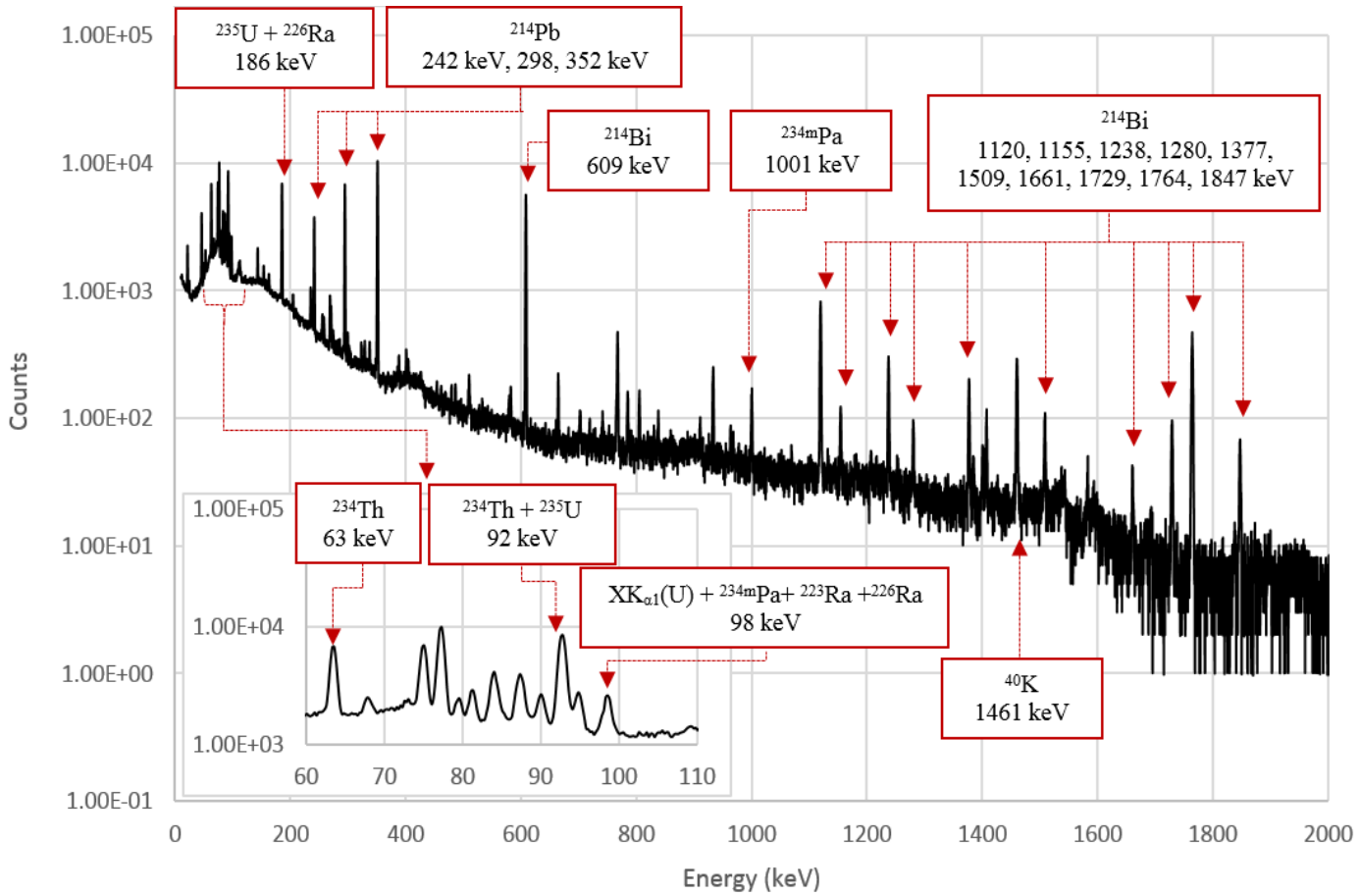

Fig. 1. Experimental spectrum of a 479 g ore sample with an uranium concentration of 419 ppm_U and a density of 1.46 $g.cm^{-3}$ with for 7503 seconds of acquisition

B. Radioactive gamma emission at 1001 keV

Equation (1) allows converting the net area of the 1001 keV peak into uranium mass concentration in ppm (i.e. in mg of uranium per kg of ore, dimensionless unit). This equation has been already used and validated during a measurement campaign in Bessines (France) calibration facility [3].

$$Cm_u(1001\ \text{keV}) = \frac{S_n(1001\ keV)}{Tc \times M_S \times CE_{1001}} \quad (1)$$

Where :

$$CE_{1001} = \frac{Eff_{1001keV} \times I_{1001keV}(^{234m}_{91}Pa) \times Na \times \ln(2)}{(1+\eta) \times 10^6 \times M(^{238}_{92}U) \times T_{\frac{1}{2}}(^{238}_{92}U)}$$

With:

- $Cm_u(1001\ \text{keV})$: uranium mass concentration (in ppm) of the sample calculated thanks to the gamma ray at 1001 keV,
- $S_n(1001\ keV)$: net area of the peak at 1001 keV measured on the gamma spectrum after subtraction of the Compton continuum under the peak (number of counts, dimensionless number),
- Tc: acquisition "live time" (i.e. real time corrected for dead time) of the gamma spectrum (s),
- M_s : mass of the sample (g),
- $Eff_{1001keV}$: detection efficiency calculated with MCNP [4] (number of count in the full-energy peak at 1001 keV per photon of 1001 keV emitted in the sample),
- $I_{1001keV}(^{234m}_{91}Pa)$: intensity of the 1001 keV gamma ray of ^{234m}Pa (number of gamma radiation emitted per disintegration: 0.847 % [5]) in the ^{238}U decay chain,
- Na: Avogadro constant (6,023·10^{23} atoms per mole, dimensionless number),
- η: mass fraction of ^{235}U in natural uranium (0.72 %),
- $M(^{238}_{92}U)$: molar mass of ^{238}U (g),
- $T_{\frac{1}{2}}(^{238}_{92}\text{U})$: ^{238}U radioactive period (4.5 10^9 a ≡ 141.0 10^{15} s).

C. Radioactive gamma and X-ray emissions at 92 keV

The "92 keV" peak is already used in ORANO Mining laboratories for fast uranium characterization. It is composed of close-in-energy lines mainly due to ^{235}U and ^{234}Th:

❶ the α-decay of ^{235}U towards ^{231}Th is followed by the emission of a thorium X-ray at 93.35 keV, after internal conversion of the excited ^{231}Th daughter. This X-ray contributes to the signal at 92 keV due to the finite resolution of the detector, with a tabulated emission intensity $I_{93keV}(^{235}_{92}U) = 5.75\ \%$ [5],

❷ ^{234}Th (in the beginning of the ^{238}U decay chain) emits two gamma rays at 92.38 keV and 92.80 keV following its β^- radioactive decay into ^{234}Pa. We use here the total intensity $I_{92keV}(^{234}_{90}Th) = 4.33\%$ [5],

As ^{235}U and ^{234}Th are located at the top of the uranium decay chains, the net area of the 92 keV peak is not subject to potential imbalances and correctly reflects the uranium concentration.

Equation (2) allows converting the net area of the 92 keV peak into uranium mass concentration.

$$Cm_U(92\ keV) = \frac{S_n(92\ \text{keV})}{Tc \times M_{ech} \times CE_{92}} \quad (2)$$

Where:

- $CE_{92} = CE_{^{234}_{90}Th} + CE_{^{235}_{92}u}$
- $CE_{^{234}_{90}Th} = \frac{Eff_{92keV} \times I_{92keV}(^{234}_{90}Th) \times \ln(2) \times \mathcal{N}a}{1.0072 \times 10^6 \times M(^{238}_{92}U) \times T_{\frac{1}{2}}(^{238}_{92}U)}$
- $CE_{^{235}_{92}u} = \frac{\frac{A(^{235}_{92}U)}{A(^{238}_{92}U)} \times Eff_{93keV} \times I_{93keV}(^{235}_{92}U) \times ln(2) \times \mathcal{N}a}{(1+\eta) \times 10^6 \times M(^{238}_{92}U) \times T_{\frac{1}{2}}(^{238}_{92}U)}$

With:

- $Cm_U(92\ keV)$: uranium mass concentration in ppm of sample calculated thanks to the 92 keV ray,
- Tc : acquisition "live time" (i.e. real time corrected for dead time) of the gamma spectrum (s),
- M_s : mass of the sample (g),
- $S_n(92\ \text{keV})$: net area of the peak at 92 keV (number of counts, dimensionless number),
- $I_{92keV}(^{234}_{90}Th)$: total intensity of the two 92 keV close peaks of ^{234}Th (4.33 % [5]), in the ^{238}U decay chain,
- $Eff_{92\ \text{keV}}, Eff_{93\ \text{keV}}$: detection efficiency calculated with MCNP (number of count in the full-energy peak at 92 keV or 93 keV, respectively per photon of 92 keV or 93 keV emitted in the sample),
- $\frac{A(^{235}_{92}U)}{A(^{238}_{92}U)}$: activity ratio of ^{235}U and ^{238}U (0.046 in case of natural enrichment, i.e. 0.72 % of ^{235}U),
- $I_{93keV}(^{235}_{92}U)$: emission intensity at 93 keV of ^{235}U (5.75% [5]).

D. Radioactive emission at 98 keV

The 98 keV peak is dominated by four contributions:

❶ the X-$K_{\alpha 1}$ fluorescence line of uranium at 98.44 keV. The net area of this peak does not follow linearly uranium concentration, contrary to the above radioactive-decay emissions, but it rises in a quadratic way because of the combined increase of fluorescence source intensity (gamma emitters of the uranium chain) and uranium quantity itself (which undergoes fluorescence).
❷ the same 98.44 keV X-ray but emitted after the β^- disintegration of ^{234m}Pa (at the beginning of the ^{238}U decay chain) into ^{234}U, followed by internal conversion. The tabulated emission intensity is $I_{98keV}(^{234m}_{91}Pa) = 0.316$ %,
❸ two close 97.53 keV and 97.85 keV X-rays linked to ^{223}Ra (^{235}U decay chain) α-decay into ^{219}Rn, followed by internal conversion of the excited daughter^{219}Rn. The tabulated total intensity for these two X-rays is $I_{92keV}(^{223}_{88}Ra) = 2.72$ % [5],
❹ the same 97.53 keV and 97.85 keV X-rays but linked to ^{226}Ra (^{238}U decay chain) α-decay towards ^{222}Rn, again followed by internal conversion. The tabulated total intensity is here $I_{92keV}(^{226}_{88}Ra) = 0.036\%$ [5].

Concerning the first contribution, each gamma ray emitted by the uranium decay chain can cause the fluorescence of uranium after undergoing Compton scattering and photoelectric absorption in the sample. In order to quantify the ability of a photon of energy E to induce uranium fluorescence, the $\eta_{fluo}(E)$ yield defined in equation (3) is calculated by MCNP (in g^{-1} units). This fluorescence yield is specific to the geometry of the sample: uranium content, filling height, density, mineralogy.

$$\eta_{fluo}(E) = \frac{S_n(XK_{\alpha 1})}{S_n(E) \times \text{Cm}_\text{U} \times M_s} \quad (3)$$

With:

- $S_n(XK_{\alpha 1})$: net area of the $XK_{\alpha 1}$ fluorescence line of uranium at 98.4 keV (number of counts, dimensionless number),
- $S_n(E)$: net area, on the MCNP spectrum, at the simulated energy E (number of counts, dimensionless number),
- Cm_U: uranium mass concentration (in ppm) in the MCNP model of the sample,
- M_s : mass of the sample (g).

A typical fluorescence yield calculation with a mono-energy 200 keV photon is shown in Fig. 2.

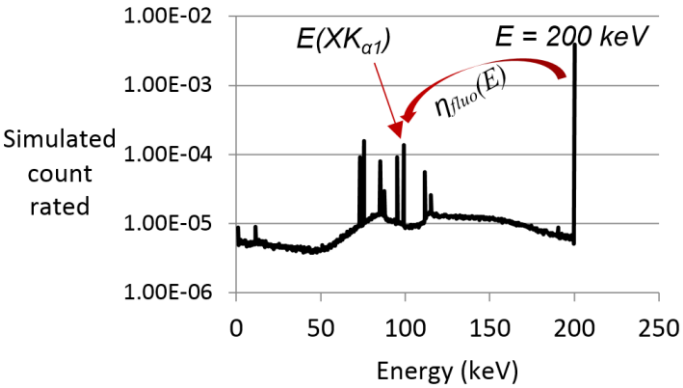

Fig. 2. Gamma spectrum and induced fluorescence X-rays for a 200 keV mono-energy photon source.

The fluorescence yield and the three radioactive decay emissions listed above allow us to convert the net area of the 98 keV peak into a uranium mass concentration using equation (4). It is important to notice that, in order to limit the number of simulations, only the six more intense gamma rays were taken into account to calculate the fluorescence yield: 185 keV (^{214}Pb), 242 keV (^{214}Pb), 298 keV (^{214}Pb), 352 keV (^{214}Pb), 609 keV (^{214}Bi) and 1120 keV (^{214}Bi). As they represent 78 % of the total fluorescence signal, a correction factor F equal to 0.78 is used in equation (4).

$$Cm_U(98\ keV) = \frac{S_n(98\ \text{keV})}{Tc \times M_s \times CE_{98}} \quad (4)$$

Where:

- $CE_{98} = CE_{^{226}_{88}Ra} + CE_{^{223}_{88}Ra} + CE_{^{234m}_{91}Pa} + \frac{\sum_{E_\gamma}\left[\eta_{fluo}(E_\gamma,d,h) \times S_n(E_\gamma)\right]}{Tc \times \text{F}}$
- $CE_{^{226}_{88}Ra} = \frac{\frac{A(^{226}_{88}Ra)}{A(^{238}_{92}U)} \times Eff_{98keV} \times I_{98keV}(^{226}_{88}Ra) \times ln(2) \times \mathcal{N}a}{(1+\eta) \times 10^6 \times M(^{238}_{92}U) \times T_{\frac{1}{2}}(^{238}_{92}U)}$

- $CE_{^{223}_{88}Ra} = \frac{\frac{A(^{223}_{88}Ra)}{A(^{238}_{92}U)} \times Eff_{98keV} \times \ln(2) \times Na \times I_{98keV}(^{223}_{88}Ra)}{(1+\eta) \times 10^6 \times M(^{238}_{92}U) \times T_{\frac{1}{2}}(^{238}_{92}U)}$
- $CE_{^{234m}_{91}Pa} = \frac{Eff_{98keV} \times I_{98keV}(^{234m}_{91}Pa) \times ln(2) \times Na}{(1+\eta) \times 10^6 \times M(^{238}_{92}U) \times T_{\frac{1}{2}}(^{238}_{88}U)}$

With:

- $Cm_U(98\ keV)$: uranium mass concentration (in ppm) of the sample calculated thanks to the 98 keV ray,
- Tc: acquisition "live time" (i.e. real time corrected for dead time) of the gamma spectrum (s),
- M_s : mass of the sample (g),
- $S_n(98\ \text{keV})$: net area of the peak at 98 keV (number of counts, dimensionless number),
- Eff_{98keV} : detection efficiency calculated with MCNP (number of count in the full-energy peak at 98 keV per photon of 98 keV emitted in the sample),
- $I_{98keV}(^{223}_{88}Ra)$: emission intensity at 98 keV of ^{223}Ra (2.72 % [5]),
- $I_{92keV}(^{226}_{88}Ra)$: emission intensity at 98 keV of ^{226}Ra (0.0351% [5]),
- $I_{92keV}(^{234m}_{91}Pa)$: emission intensity at 98 keV of ^{234m}Pa (0.316% [5]),
- E_γ = [185, 242, 295, 352, 609, 1120 keV], energy of the 6 gamma rays selected to calculate the fluorescence yield,
- $\eta_{fluo}(E,d,h)$: fluorescence yield (in g^{-1}) as a function of gamma energy, sample density and filling height,
- $\frac{A(^{223}_{88}Ra)}{A(^{238}_{92}U)}$: activity ratio between ^{223}Ra and ^{238}U (0.046 in the case of natural enrichment in ^{235}U),
- F: correction factor to take into account the limited number the lack of gamma rays modeled in the fluorescence source (here F = 0.78).

III. Experimental qualification

In order to validate the new approach described above, we use 76 gamma spectra of uranium ore samples recorded by ORANO Mining (such as the spectrum of Fig. 1) to study radioactive disequilibrium in Dulann Uul and Zoovch Ovoo deposits, Mongolia [2]. The samples have different densities and filling heights. The uranium ore was coarsely crushed with a hammer and placed in a flask, as shown in Fig. 3. The crushed samples have an average density of 1.4 g.cm^{-3}. The average filling height is 6 cm and the sample holder diameter is 11 cm. The sample is placed on PVC shims of variable height to ensure the contact between the detector cover and the ore sample. In addition, a copper shielding was used to absorb fluorescence X- rays of the lead shielding (Fig. 3). The BEGE 2830 planar HPGe crystal of the FALCON 5000 handheld detector (from MIRION-CANBERRA) has a 60 mm diameter and a 30 mm length. In order to calculate the fluorescence yield, the measurement geometry was modeled with MCNP6 Monte-Carlo transport code [4], see Fig. 3.

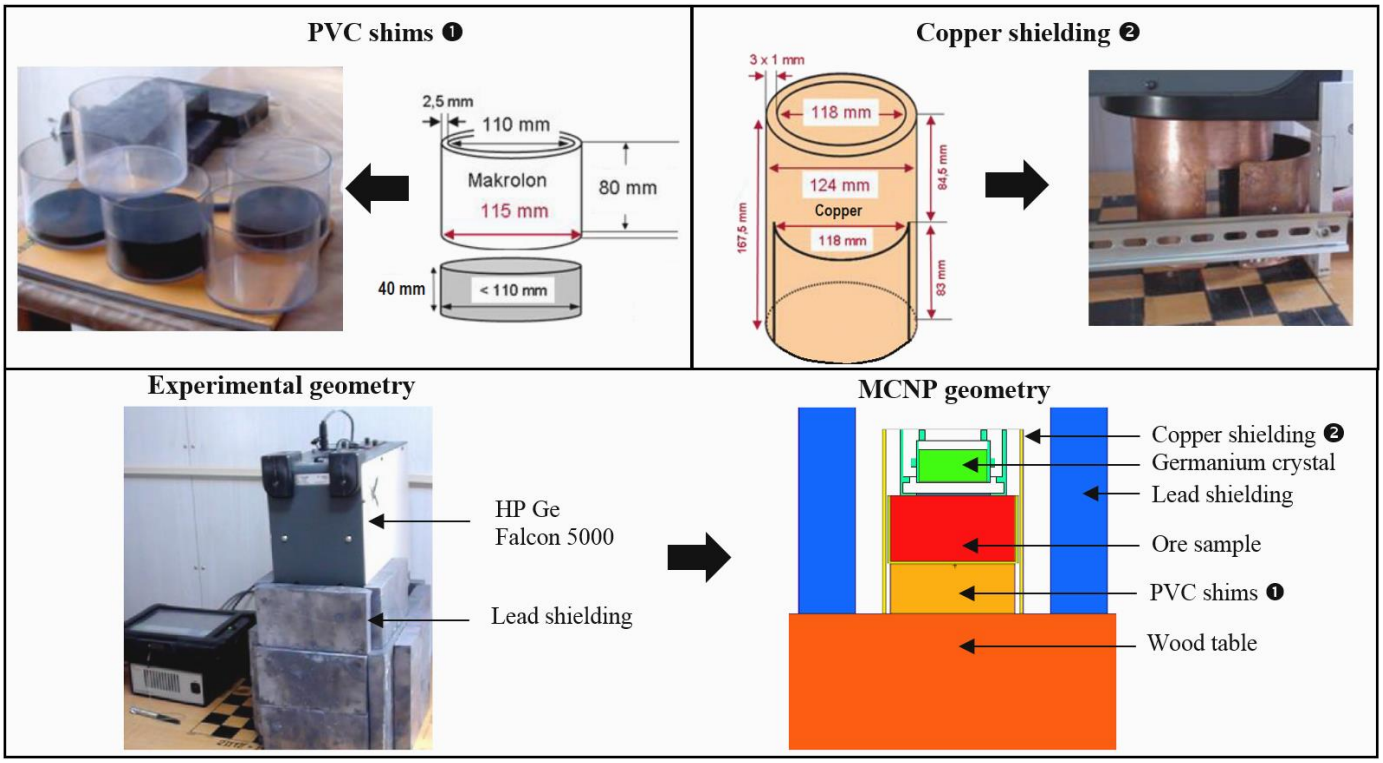

Fig. 3. Experimental and simulated geometry. On the upper left side, the PVC shims. On the upper right side, the copper shielding. At the bottom, the experimental geometry and the MCNP geometry.

Efficiencies at 92 keV, 98 keV and 1001 keV are those calculated with ISOCS software [6] for a typical FALCON 5000 geometry. The uncertainty associated to calculated efficiencies is 10 % for 92 keV and 98 keV peaks and 5 % for 1001 keV peak.

The following graph represents the $Cm_U(92\ keV)$ and $Cm_U(98\ keV)$ concentrations calculated with the net area of the 92 keV and 98 keV peaks, respectively, as a function of the concentration calculated with the 1001 keV peak, which is considered as the reference.

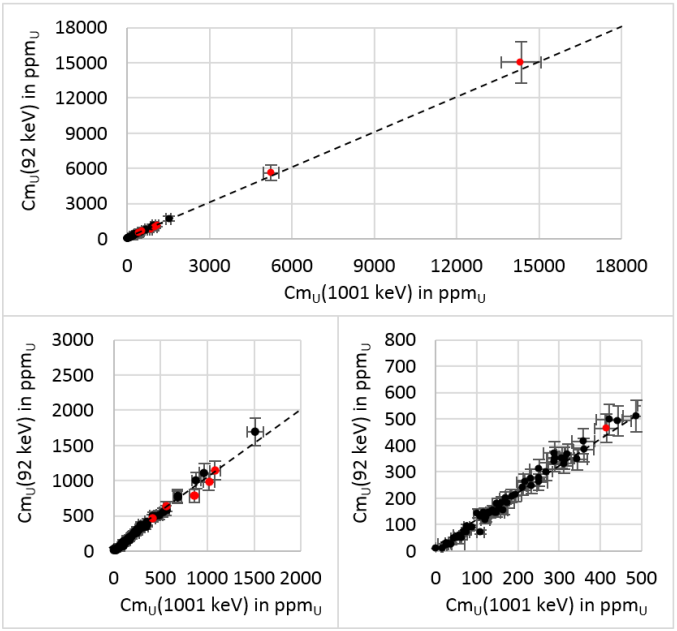

Fig. 4. Uranium content $Cm_U(92\ keV)$ as a function of $Cm_U(1001\ keV)$.

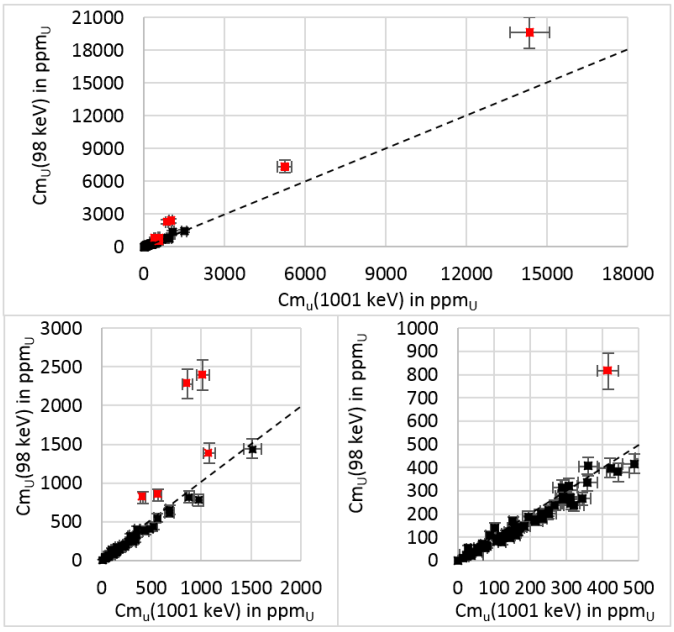

Fig. 5. Uranium content $Cm_U(98\ keV)$ as a function of $Cm_U(1001\ keV)$.

The uncertainty calculated for each sample (considered as homogeneous) includes:

- detector calibration and detection efficiency calculation by ISOCS [6],
- the statistical uncertainty on the net area of the 1001 keV, 92 keV and 98 keV peaks,
- the relative uncertainties on the intensities of the gamma or X-rays of interest are given in the nuclear databases [5]: 0.94 % for the 1001 keV gamma ray; for the 92 keV peak it is 6.21% for the ^{234}Th contribution and 1.91 % for ^{235}U part; for the 98 keV line, it is 1.26 % for ^{234m}Pa, 2.85 % for ^{226}Ra, and 2.57% for ^{223}Ra,
- the relative uncertainty on the fluorescence yield simulated for the calculation of $Cm_U(98\ keV)$ is estimated to be around 20 % for the six modeled gamma emissions,
- the relative uncertainty on the F = 0.78 correction factor (for the non-modeled gamma rays inducing about 22 % of the fluorescence) is estimated to be 5% based on several simulations with different samples.

An average relative uncertainty of 10.34 % is thus calculated for $Cm_U(1001\ keV)$, 11.69 % for $Cm_U(92\ keV)$ and 12.85% for $Cm_U(98\ keV)$. The uncertainty on $Cm_U(1001\ keV)$ is mainly due to the poor counting statistics, leading to large uncertainties in both the Gaussian adjustment of the gamma ray (broadened by the detector resolution) and in the estimation of the Compton continuum under the peak. Concerning $Cm_U(92\ keV)$ and $Cm_U(98\ keV)$ the relative uncertainty on the efficiency calculated with ISOCS software dominates (10 %). It could be reduced by using a MCNP refined detector model based on a fine geometrical characterization with collimated calibration sources, which will be reported in a future article. For most of the 76 samples, $Cm_U(92\ keV)$ and $Cm_U(98\ keV)$ are consistent with the reference $Cm_U(1001\ keV)$, but for seven samples (in red on Fig. 4 and Fig. 5), discrepancies are observed that might be due to heterogeneities. Indeed, for all these samples, we observe the following inequality:

$$Cm_U(98\ keV) > Cm_U(1001\ keV) \geq Cm_U(92\ keV)$$

As explained above, in case of uranium nuggets in the sample, X and gamma emissions following radioactive decays are more self-absorbed than with a uniform distribution, while on the contrary, X-ray fluorescence is enhanced. This phenomenon was demonstrated by simulating with MCNP a uranium nugget of 0.343 g_U in a homogeneous matrix of uranium of 0.455 g_U. This simulation, equivalent of a homogeneous sample of 1000 ppm_U, gives $Cm_U(92\ keV)$ = 690 ppm_U and $Cm_U(98\ keV)$ = 3645 ppm_U.

Beyond detection of possible heterogeneities, the advantage of the method is to reduce measurement time. The gain in measurement time was calculated for each sample by comparing the statistical uncertainty of the 1001 keV with that of 92 keV and 98 keV peaks, taking in account the estimation and subtraction of the Compton continuum under the peaks. Than the gain in measurement time is estimated with the aim to have the same relative uncertainty in the 92 and 98 keV lines, during a short acquisition, as in the 1001 keV line during the long acquisition. In other words, based on Poisson law, the ratio of the 1001 keV relative uncertainty to that of 92 or 98 keV lines is squared to be converted in time gain. The average gain

is 65 for $Cm_U(92\ keV)$ and 2 for $Cm_U(98\ keV)$, but they vary a lot for each sample depending of many factors such as geometry, uranium content and possible radioactive disequilibrium in the uranium chain. For instance, no gain is observed for $Cm_U(98\ keV)$ for very small uranium contents (namely less than 200 ppm_U) because self-fluorescence if too weak. On the other hand, for large uranium contents, the gain for $Cm_U(98\ keV)$ increases quickly because, as explained above, the intensity of fluorescence X-ray rises with the square of uranium concentration. For instance, the gain in measurement time for the highest uranium content sample (14,000 ppm) is about 8 for Cm_U(98 keV).

The gain for Cm_U(92 keV) fluctuates from one sample to another, but it is little dependent on uranium concentration in this range. In addition, if sample homogeneity is guaranteed (e.g. thanks to fine crushing), the time gain is a factor 70 by using the 92 keV line only, as heterogeneity detection with the 98 keV peak is no more necessary.

IV. CONCLUSION AND PROSPECTS

In this work, we have shown the possibility to measure the uranium concentration of uranium ore samples by gamma-ray spectroscopy using the 92 keV and 98 keV lines, which lead to a large measurement time gain (minutes vs. hours) compared to the reference 1001 keV peak. The total relative uncertainty on $Cm_U(92\ keV)$ and $Cm_U(98\ keV)$ mass concentrations measured in a short acquisition remains lower than 13 %, while it was about 10 % for the long measurement of $Cm_U(1001\ keV)$.

In addition, a difference in the uranium concentrations assessed with the 92 and 98 keV peaks, respectively, alerts the operator of a possible heterogeneity of the sample.

In next studies, the geometric MCNP model of the Falcon 5000 detector will be optimized to reduce the uncertainty on $Cm_U(92\ keV)$ and $Cm_U(98\ keV)$, which is so far dominated by modeling uncertainty. This detector is equipped with a planar HPGe crystal, which will be finely characterized with a multi-energy highly collimated ^{152}Eu gamma source. This narrow photon beam will allow precisely estimating the dead layers vs. active area of the germanium crystal [3].

We will also measure 38 additional ore samples provided by ORANO Mining, on a wider range of uranium concentrations, to fully qualify the method in the Nuclear Measurement Laboratory of CEA, DEN, Cadarache.

In parallel, we also study a low-resolution spectroscopy approach with easy-to-use room temperature NaI(Tl) or $LaBr_3$(Ce) detectors, reducing again measurement time, and system cost as well.

REFERENCES

[1] "Falcon 5000 Portable HPGe-Based Radionuclide Identifier." [Online]. Available: https://www.mirion.com/products/falcon-portable-hpge-based-radionuclide-identifier. [Accessed: 22-Jan-2019].

[2] T. Boulesteix *et al.*, "Ilmenites and their alteration products, sinkholes for uranium and radium in roll-front deposits after the example of South Tortkuduk (Kazakhstan)," vol. To be published.

[3] T. Marchais *et al.*, "Detailed MCNP Simulations of Gamma-Ray Spectroscopy Measurements With Calibration Blocks for Uranium Mining Applications," *IEEE Trans. Nucl. Sci.*, vol. 65, no. 9, pp. 2533–2538, Sep. 2018.

[4] "MCNP6TM, User's manual – Version 1.0 - LA-CP-13-00634, Rev. 0 – May 2013 – Denise B. Pelowitz, editor." Los Alamos National Laboratory.

[5] "NUCLÉIDE-LARA on the web (2018)." [Online]. Available: http://www.nucleide.org/Laraweb/index.php. [Accessed: 22-Jan-2019].

[6] MIRION Technologies, "ISOCS– Model S573 ISOCS, Calibration Software." Apr-2013.